IEEE Access
Multidisciplinary | Rapid Review | Open Access Journal

Received 1 September 2022, accepted 8 September 2022, date of publication 12 September 2022,
date of current version 21 September 2022.

Digital Object Identifier 10.1109/ACCESS.2022.3206386

RESEARCH ARTICLE

Modulated Dual-Voltage-Vector Model-Free Predictive Current Controller for Synchronous Reluctance Motor Drives With Online Duty Cycle Calculation

VENKATA R. REDDY[1], CRESTIAN ALMAZAN AGUSTIN[2], (Graduate Student Member, IEEE), CHENG-KAI LIN[3], AND JUNG-CHIEH CHEN[3]

[1]Department of Electrical and Electronics Engineering, SRM University, Amaravati, Andhra Pradesh 522502, India
[2]Department of Electrical Engineering, Isabela State University, Ilagan Campus, Ilagan, Isabela 3300, Philippines
[3]Department of Electrical Engineering, National Taiwan Ocean University, Keelung 202301, Taiwan

Corresponding author: Cheng-Kai Lin (cklin@mail.ntou.edu.tw)

This work was supported by the National Science and Technology Council, Taiwan, under Grant NSTC-111-2221-E-019-025.

ABSTRACT In this paper, a modulated dual-voltage-vector model-free predictive current control with online duty cycle calculation is proposed and applied to drive a synchronous reluctance motor. The dual-voltage-vector modulation scheme reduces the current ripples and errors in the single-voltage-vector method. The proposed method reduces the predictive current controller's calculation time by first setting the initial value of the duty cycle to a constant. Then, an optimal switching mode can be selected by minimizing a cost function. Next, the required duty cycle can be calculated directly by the proposed method without any differential calculations instead of its initial value. The proposed method can effectively track the stator current, reducing the maximum average current error by 34.8% compared to the conventional single-voltage-vector scheme. Finally, the correctness and feasibility of the modulated model-free predictive current controller with the online duty cycle calculation proposed in this article are verified by the experimental results using Texas Instruments microcontroller TMS320F28379D.

INDEX TERMS Dual-voltage-vector, modulated model-free predictive current controller, online duty cycle calculation, synchronous reluctance motor.

I. INTRODUCTION

In recent years, synchronous reluctance motor (SynRM) drives in industrial and commercial applications have rapidly increased [1]. The unique nature of its rotor construction, where no winding and embedded permanent magnets, makes the SynRM commercially viable and advantageous over other motor drives [2]. A few advantages of the SynRM are easy to operate in wide speed ranges, high power density, reduced noise and vibrations, and increased reliability [3]. Moreover, without magnetic materials, induced currents are eliminated, and losses are reduced, making the system simple and more efficient [4], [5]. The advantages mentioned above and features establish the SynRM as the future of AC machines [6].

For the SynRM drive system to provide a better performance, fast transient response, and excellent steady-state response, controlling the motor drive system plays an important role. Generally, an inverter is used to control the motor drive systems. So, selecting an efficient control strategy for the inverter will help to obtain the motor's required features. Model predictive current control (MPCC) is one of the most popular and suitable control strategies for motor drive applications [7], [8]. MPCC has drawn significant attention due to its simplicity, fast dynamic response, and nonlinear control flexibility [9]. However, implementation of this

The associate editor coordinating the review of this manuscript and approving it for publication was Justin Zhang.

method involves a large amount of computation, whereas the conventional control method does not. However, with the advent of powerful high-speed microcontrollers, the problem of large and complex computational requirements is ruled out.

J. Rodriguez *et al.* applied the MPCC to the voltage source inverter [10], which can predict the optimal voltage switching vector of the inverter. Its principle is majorly dependent on predicting future currents based on the mathematical model of the load. Therefore, the accuracy of the predicted current and the performance of the controller depend on motor parameters like flux linkage, q-axis inductance, resistance, and extended back-emf. MPCC has been applied effectively in SynRM for various control objectives like torque, flux, current, and speed [11], [12]. Despite MPCC's excellent performance, the parameter uncertainties and dependence on model parameters can degrade the efficacy of the system. MPCC with gray prediction was developed in [13] to deal with parameter uncertainties, which delivers good current response and anti-interference ability. On the other hand, this method involves high computation and is time-consuming. In [14], an adaptive disturbance observer method was developed to decrease the mismatch in inductance and reduce the current oscillations. However, this method does not consider the mismatches in flux and resistance. An enhanced stator current and disturbance observed method was implemented in [15] to overcome the challenges of system stability during parameter mismatches. Nevertheless, it requires adjusting and selecting reasonable sliding parameters due to noise. In addition, the scheme is also dependent on motor parameters. A model predictive current controller based on a reduced-order observer is proposed in [16], which can observe and compensate for lumped disturbances with a lesser computational burden. However, the controller performance deteriorates when parameter mismatches exist due to aging, temperature, or other faults.

To reduce the influence of parameter uncertainty on the current tracking performance model-free predictive current controller (MFPCC) is proposed in [1] and [17]. This method operates without using the motor parameters and is suitable for different motor drive applications. It predicts the future currents based on the previously stored stator currents, which helps eliminate the requirement for a system model and dependency on motor parameters in the controller. Minimal attempts are made to employ MFPCC to SynRM drives [1], [18] and are operated with a conventional single input voltage vector. Implementing a single-voltage-vector (SVV) in each switching cycle makes it more difficult to eliminate or reduce the current ripples and errors [19]. Modulated MPCC is developed in [20] to reduce the current ripples for a seven-level H-bridge converter. Multiple voltage vectors are applied in each control cycle to decrease the current ripples and current errors. Although the experimental studies show significant improvements, these methods heavily rely on the mathematical modeling of the system and motor parameters.

In the field of predictive current controllers, increasing the switching states may raise the number of optional state combinations. It relatively increases the probability of executing the optimal switching mode or the time taken to modulate multiple voltage vectors in the same prediction period. Therefore, methods such as increasing the number of optional voltage vectors can be better than the existing SVV predictive current control in current tracking performance, reducing current error and ripple, lowering total harmonic distortion rate, and having other advantages. Therefore, this article discusses the application of modulated two-voltage-vector or dual-voltage-vector (DVV) MFPCC for SynRM drive applications. The switching strategy is first to select the average duty cycle to modulate the best switch for the voltage vector and then adjust the duty cycle to control online, which is expected to reduce the amount of calculation. It has the advantage of an excellent current tracking effect. In [21] and [22], an MPCC with duty cycle control is proposed for permanent magnet synchronous hub motor drives. Unlike the proposed method, the developed duty cycle and control scheme strategy depends upon motor parameters, influencing the system's performance.

Unlike the SVV-based predictive current controllers, the DVV follows the predictive current control to pursue the optimal switching state during the sampling period. It has the optimal time-proportion modulation with time-varying characteristics, and relatively speaking, the switching state is also modulated due to the time-proportion modulation. The selectable range of the voltage vector is also refined from a single point to several line segments, allowing more freedom in selecting voltage vectors. In different vector numbers, the cost function is the criterion for predicting the current control to select the best switching mode. The difference in the design of this cost function affects the benchmark for choosing the best switching mode and the application time ratio.

For the application time ratio, the proposed prediction current control with an online duty cycle calculation modulation changes the cost function, thereby omitting the need to use many calculations in the time ratio. The proposed method increases the computational burden and reduces the average current error compared to the SVV. There is a trade-off between the computational burden and average current error. However, with the development of advanced microprocessors higher computational burden will not be a problem. All 25 groups of switching combinations of the DVV modulation scheme are calculated, and online duty cycle modulation is performed after selecting the optimal switching mode. The design first modulates the voltage vector with the same duty cycle to obtain the optimal switch combination. Then, design and calculate the online duty cycle with this combination. The proposed method provides an excellent current tracking effect and can significantly reduce execution time. The main contributions of the article are as follows:

1. A novel modulated dual-voltage-vector MFPCC with online duty-cycle calculation for a synchronous reluctance motor drive is proposed.

2. Online duty ratio calculation reduces the calculation time and cost function.
3. The proposed method reduces the current ripples and errors compared to the conventional single-voltage-vector one; it also reduces calculation time.
4. Experimental studies under steady-state and transient conditions are performed in different operating conditions. Furthermore, a detailed comparison study is performed with SVV MFPCC.

The rest of the article is organized as follows. The implementation details of the proposed modulated dual-voltage-vector with online duty cycle calculation are given in Section II. The cost function and application time ratio are also calculated in this section. The practical validation and performance evaluation of the proposed method is given in Section III. The performance of the proposed method is also compared with modulated SVV MFPCC. A detailed quantitative analysis is also performed. Finally, conclusions are provided in Section IV

II. MODULATED DUAL-VOLTAGE-VECTOR MODEL-FREE PREDICTIVE CURRENT CONTROL

A. MODULATED DUAL-VOLTAGE-VECTOR

Conventional modulation schemes generally select a single-voltage vector for each switching cycle. However, recent studies show that using only one voltage vector in the modulation scheme increases the current ripples and errors [19]. This section explains the implementation of DVV modulation using MFPCC for SynRM. The proposed method can eliminate the disadvantages above by increasing the input voltage vectors in each switching cycle. The mathematical modeling of SynRM is presented by many researchers [1], [3], [5], [6]. This paper does not describe the mathematical modeling of SynRM to avoid repetition. Moreover, in the proposed modulated MFPCC, the mathematical model of the SynRM is not required. The proposed modulated DVV is explained as follows.

The dual-voltage-vector modulation is formed by modulating two sets of voltage vectors in proportion to time, as shown in Fig. 1. In the figure $v_1^m \sim v_6^m$ are the modulations of the non-zero single-voltage vector and the zero-voltage vector; $v_7^m \sim v_{24}^m$ are the modulations of two non-zero single-voltage vectors; the superscript "m" represents the symbol of the dual-voltage-vector modulation, and the modulation is expressed in the form of a line segment in the voltage vector diagram.

The application time of the dual-voltage-vector is defined as:

$$T^{m1} + T^{m2} = T_s, \quad T^{m1},\ T^{m2} \in [0, T_s] \tag{1}$$

The superscript symbols "*m1*" and "*m2*" are the first and second order of application of the voltage vectors, respectively; hence, T^{m1} and T^{m2} denotes the first and second applied voltage vectors of the dual-voltage vector modulation application time. The proportion of the application time of the

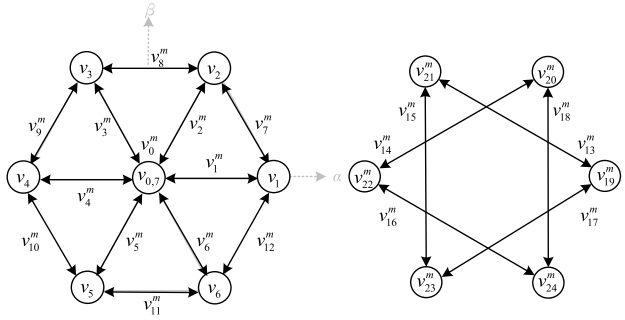

FIGURE 1. Voltage vector diagram of modulating two voltage vectors.

dual-voltage-vector in the prediction period is further defined as:

$$D^{m1} + D^{m2} = 1, \quad D^{m1},\ D^{m2} \in [0, 1] \tag{2}$$

$$D^{mp} = \frac{T^{mp}}{T_s}, \quad p \in \{1, 2\} \tag{3}$$

where D^{m1} and D^{m2} denote the first and second applied duty ratios, respectively. They correspond to the dual-voltage-vector modulation's first and second voltage vectors in the prediction period. The application time ratio must be limited to the [0,1] interval. To meet the actual situation, the limits must be observed so that the optimal application time ratio can be calculated within the interval. The synthesized dual-voltage vector obtained through modulation is given as:

$$v_n^m = D^{m1} v^{m1} + D^{m2} v^{m2}, \quad n \in \{0, 1, 2, 3, \ldots., 24\} \tag{4}$$

where v_n^m is any of the synthesized voltage vector modulated by the dual voltage vectors; v^{m1} and v^{m2} respectively refer to the first and second applied voltage vectors, which correspond to any of the fundamental voltage vectors, *i.e.*, $v^{m1}, v^{m2} \in \{v_0, v_1, \ldots\ldots, v_6\}$. Table 1 shows the relationship between the switching state combination and DVV after modulation and synthesis. In the given table, $S_0^m, S_1^m, \ldots\ldots, S_{24}^m$ correspond to the combinations of switching states of the dual-voltage-vector modulation; S^{m1} and S^{m2} represent the first and second switching states of the dual-voltage-vector modulation.

The duty cycle of the voltage vector modulation will inevitably increase the calculation amount of the microprocessor. To reduce the execution time of the algorithm and maximize its computing limit, we design a modulation strategy with online duty cycle calculation. This can be accomplished using a two-step design approach and is given as follows: Firstly, the voltage vector modulation is performed on the switching combination, and the application time ratio can be obtained from the average number of voltage combinations in the prediction period. According to equation (1), the voltage vector of this combination is calculated and modulated with an online duty cycle, allowing the optimal application time ratio and performing duty cycle modulation for the optimal switching state. The

TABLE 1. Relationship of dual-voltage-vectors after modulation and synthesis.

Line Segment	Switching State/ Composite Vector	Switching State Combination		Resulting Linear Combination
		S^{m1}	S^{m2}	
0	S_0^m, v_0^m	S_0 (000)	S_0 (000)	$v_0^m = D^{m1}v_0^{m1} + D^{m2}v_0^{m2}$
1	S_1^m, v_1^m	S_1 (100)	S_0 (000)	$v_1^m = D^{m1}v_1^{m1} + D^{m2}v_0^{m2}$
2	S_2^m, v_2^m	S_2 (110)	S_0 (000)	$v_2^m = D^{m1}v_2^{m1} + D^{m2}v_0^{m2}$
3	S_3^m, v_3^m	S_3 (010)	S_0 (000)	$v_3^m = D^{m1}v_3^{m1} + D^{m2}v_0^{m2}$
4	S_4^m, v_4^m	S_4 (011)	S_0 (000)	$v_4^m = D^{m1}v_4^{m1} + D^{m2}v_0^{m2}$
5	S_5^m, v_5^m	S_5 (001)	S_0 (000)	$v_5^m = D^{m1}v_5^{m1} + D^{m2}v_0^{m2}$
6	S_6^m, v_6^m	S_6 (101)	S_0 (000)	$v_6^m = D^{m1}v_6^{m1} + D^{m2}v_0^{m2}$
7	S_7^m, v_7^m	S_1 (100)	S_2 (110)	$v_7^m = D^{m1}v_1^{m1} + D^{m2}v_2^{m2}$
8	S_8^m, v_8^m	S_2 (110)	S_3 (010)	$v_8^m = D^{m1}v_2^{m1} + D^{m2}v_3^{m2}$
9	S_9^m, v_9^m	S_3 (010)	S_4 (011)	$v_9^m = D^{m1}v_3^{m1} + D^{m2}v_4^{m2}$
10	S_{10}^m, v_{10}^m	S_4 (011)	S_5 (001)	$v_{10}^m = D^{m1}v_4^{m1} + D^{m2}v_5^{m2}$
11	S_{11}^m, v_{11}^m	S_5 (001)	S_6 (101)	$v_{11}^m = D^{m1}v_5^{m1} + D^{m2}v_6^{m2}$
12	S_{12}^m, v_{12}^m	S_6 (101)	S_1 (100)	$v_{12}^m = D^{m1}v_6^{m1} + D^{m2}v_1^{m2}$
13	S_{13}^m, v_{13}^m	S_1 (100)	S_3 (010)	$v_{13}^m = D^{m1}v_1^{m1} + D^{m2}v_3^{m2}$
14	S_{14}^m, v_{14}^m	S_2 (110)	S_4 (011)	$v_{14}^m = D^{m1}v_2^{m1} + D^{m2}v_4^{m2}$
15	S_{15}^m, v_{15}^m	S_3 (010)	S_5 (001)	$v_{15}^m = D^{m1}v_3^{m1} + D^{m2}v_5^{m2}$
16	S_{16}^m, v_{16}^m	S_4 (011)	S_6 (101)	$v_{16}^m = D^{m1}v_4^{m1} + D^{m2}v_6^{m2}$
17	S_{17}^m, v_{17}^m	S_5 (001)	S_1 (100)	$v_{17}^m = D^{m1}v_5^{m1} + D^{m2}v_1^{m2}$
18	S_{18}^m, v_{18}^m	S_6 (101)	S_2 (110)	$v_{18}^m = D^{m1}v_6^{m1} + D^{m2}v_2^{m2}$
19	S_{19}^m, v_{19}^m	S_1 (100)	S_1 (100)	$v_{19}^m = D^{m1}v_1^{m1} + D^{m2}v_1^{m2}$
20	S_{20}^m, v_{20}^m	S_2 (110)	S_2 (110)	$v_{20}^m = D^{m1}v_2^{m1} + D^{m2}v_2^{m2}$
21	S_{21}^m, v_{21}^m	S_3 (010)	S_3 (010)	$v_{21}^m = D^{m1}v_3^{m1} + D^{m2}v_3^{m2}$
22	S_{22}^m, v_{22}^m	S_4 (011)	S_4 (011)	$v_{22}^m = D^{m1}v_4^{m1} + D^{m2}v_4^{m2}$
23	S_{23}^m, v_{23}^m	S_5 (001)	S_5 (001)	$v_{23}^m = D^{m1}v_5^{m1} + D^{m2}v_5^{m2}$
24	S_{24}^m, v_{24}^m	S_6 (101)	S_6 (101)	$v_{24}^m = D^{m1}v_6^{m1} + D^{m2}v_6^{m2}$

applied voltage vector relations and synthesis can be shown in Table 1.

B. CURRENT PREDICTION

The best current sampling timing is when the preceding and following prediction intervals alternate, that is, the moment when the inverter switches are triggered. Since the time between the dead zone and surge zone is very close, the current values obtained before and after the ideal sampling point can be approximated to the current value obtained at the ideal sampling point. This method is called correction of the current sampling time point. The modulated dual-voltage-vector model-free predictive current control in the actual situation needs to correct the current sampling timing due to the correction of the current sampling time point. Moreover, the phenomenon can be associated with time-consuming

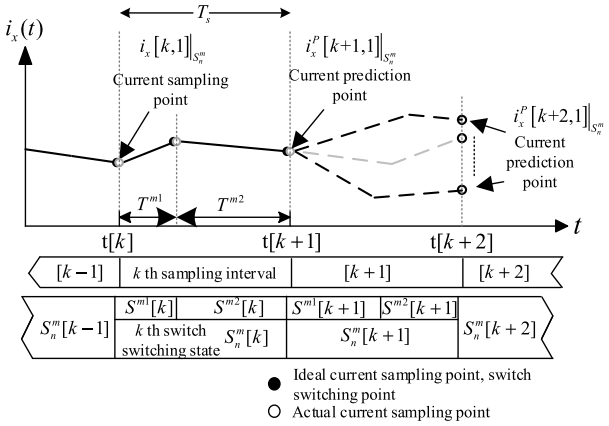

FIGURE 2. Timing diagram of modulating dual-voltage-vector after modification is implemented.

signal transmission and conversion [23]. The timing diagram is illustrated in Fig. 2.

Under the premise of an extremely short sampling period, the current change in MPCC can be regarded as linear. After each switching actuation, a current sampling is performed to obtain the current variation corresponding to each applied switching state. Then, the current variation record value is obtained as shown below:

$$\Delta i_x[k-1]|_{S_n^m[k-1]} = i_x[k]|_{S_n^m[k-1]} - i_x[k-1]|_{S_n^m[k-2]} \quad (5)$$

$$\Delta i_x^{rec}[k-1]\big|_{S_u=S_n^m[k-1]} = \Delta i_x[k-1]|_{S_n^m[k-1]}, \quad u \in \{0, 1, \ldots, 24\} \quad (6)$$

where $\Delta i_x[k-1]|_{S_n^m[k-1]}$ is the current variation of the (k-1)th time, which is obtained by subtracting the kth switching state $S_n^m[k]$ and the (k-1)th switching state $S_n^m[k-1]$; Δi_α and Δi_β are α and β axis stator change in current; the superscript "rec" is the recorded value; $\Delta i_x^{rec}[k-1]\big|_{S_u=S_n^m[k-1]}$ is the recorded value of the α- axis and β- axis current variation corresponding to the switching state of the switch $S_u \in \{S_0, S_1, \ldots, S_{24}\}$. The modulated dual-voltage-vector model-free predictive current control will be calculated according to the recorded value of the current change after sampling, and the current sampling times are equal to the applied current. The recorded value of current variation given in (5) for DVV modulation is extended as follows:

$$\Delta i_x[k-1]|_{S_n^m[k-1]} = \Delta i_x[k-1,1]|_{S^{m1}[k-1]} + \Delta i_x[k-1,2]|_{S^{m2}[k-1]} \quad (7)$$

where:

$$\Delta i_x[k-1,1]|_{S^{m1}[k-1]} = i_x[k-1,2]|_{S^{m1}[k-1]} - i_x[k-1,1]|_{S^{m2}[k-2]}$$

$$\Delta i_x[k-1,2]|_{S^{m2}[k-1]} = i_x[k,1]|_{S^{m2}[k-1]} - i_x[k-1,1]|_{S^{m1}[k-1]}$$

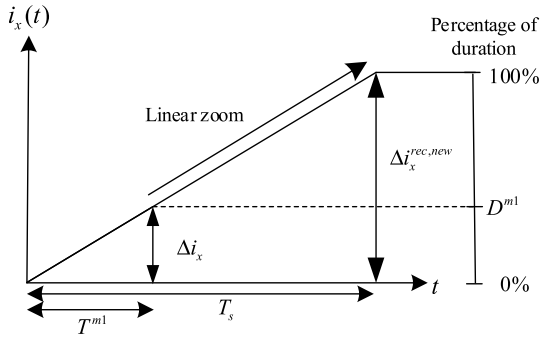

FIGURE 3. Standardized schematic diagram with sampling current.

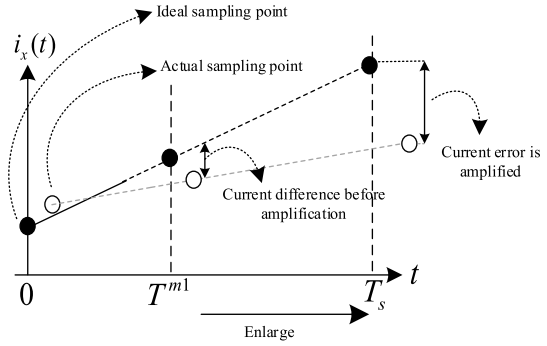

FIGURE 4. Schematic diagram of the misalignment of the recorded value.

where $\Delta i_x[k-1,1]|_{S^{m1}[k-1]}$ is the first switching state of the (k-1)th modulated two voltage vectors. In the model predictive current control technique, the current variation will not match the prediction results due to the application time of the switching state after the modulation. Therefore, it is necessary to generalize (6) to standardize the current variation, as shown in Figure 3.

$$\Delta i_x^{rec,new}\big|_{S_u=S_n^{mp}[k-1]} = \frac{\Delta i_x[k-1,p]|_{S_u=S_n^{mp}[k-1]}}{D^{mp}}, \quad p \in \{1,2\} \tag{8}$$

The superscript symbol "*rec, new*" is the annotation after the record value is updated; $\Delta i_x^{rec,new}$ is the updated record value of the α-β axes current change. However, due to the influence of correction of the current sampling time point, the standardized action of (8) will amplify the sampling error, which will lead to the inaccuracy of the recorded value of current change or variation, as shown in Figure 4.

In this article, the misalignment of the current variation is corrected by imposing the application time ratio to the recorded value and ensuring that the misalignment is within the allowable range. Accordingly, the new recorded value is modified from the following relation:

$$\Delta i_x^{rec,new}\big|_{S_u=S_n^{mp}[k-1]} = (1-D^{mp})\,\Delta i_x^{rec}\big|_{S_u=S_n^{mp}[k-1]} + \Delta i_x[k-1,p]|_{S_u=S_n^{mp}[k-1]} \tag{9}$$

Finally, the (k + 1)th stator current equation of the model-free predictive current control of dual-voltage-vector modulation with online duty cycle calculation is expressed as:

$$i_x^p[k+1,1]\big|_{S_n^m} = i_x[k,1]|_{S_n^{m2}[k-1]} + \Delta i_x[k]|_{S_u=S_n^m[k]} \tag{10}$$

The current controller considers the delay compensation to extend the prediction period to the (k + 2)th switching horizon. The stator current equation can therefore be obtained as follows:

$$i_x^p[k+2,1]\big|_{S_n^m} = i_x[k+1,1]|_{S_n^{m2}[k]} + \Delta i_x[k+1]|_{S_u=S_n^m[k+1]} \tag{11}$$

Although the (k + 1)th and (k + 2)th stator current sampling values cannot be known immediately, the current variation obtained can be calculated based on the recorded value of the current change corresponding to the switching state and application time. The expression can be approximated as:

$$\Delta i_x[k]|_{S_n^m[k]} \approx \Delta i_x^{rec}[k]\big|_{S_u=S_n^m[k]} \tag{12}$$

$$\Delta i_x[k,p]|_{S_n^m[k]} \approx D^{mp}\Delta i_x^{rec}[k,p]\big|_{S_u=S_n^{mp}[k]} \tag{13}$$

From (10), (11), and (12), the stator current prediction expression of the (k + 2)th order can be deduced as:

$$i_x^p[k+2,1]\big|_{S_n^m} = i_x[k,1]|_{S_n^{m2}[k-1]} + \Delta i_x^{rec}[k]\big|_{S_u=S_n^m[k]} + \Delta i_x^{rec}[k+1]\big|_{S_u=S_n^m[k+1]} \tag{14}$$

Recalling the identity relation of (2), we can simplify the current predicted value into an expression of an unknown variable. For instance, at (k + 1)th instant, the application time ratio can be obtained so that (14) can be converted into a single unknown variable of the first duty ratio. As a result, it can be easily expressed relative to the application time of the first switch switching state and is given as:

$$\begin{aligned} i_x^p[k+2,1]\big|_{S_n^m} = {} & i_x[k,1]|_{S_n^{m2}[k-1]} + \Delta i_x^{rec}[k]\big|_{S_n^m[k]} \\ & + \Delta i_x^{rec}[k+1,2]\big|_{S_n^{m1}[k+1]} \\ & + D^{m1}(\Delta i_x^{rec}[k+1,1]\big|_{S_n^{m1}[k+1]} \\ & - \Delta i_x^{rec}[k+1,2]\big|_{S_n^{m2}[k+1]}) \end{aligned} \tag{15}$$

With (15), the predicted currents of all 25 switching states are calculated and used to calculate each switching state's cost function to obtain the optimal one. The optimal voltage vector is used to trigger the switches in the next control period, which can be used to control the SynRM as per the actual commanded current signals.

C. CALCULATION OF COST FUNCTION AND APPLICATION TIME RATIO

The cost function needs to be calculated to find the optimal switching state that results in the lowest current error. It can be obtained by finding out the current error value from the

predicted currents and the actual currents. From (15), the current error value can be calculated as follows:

$$\begin{aligned} E_x[k+2]|_{S_n^m} &= i_x^*[k+2] + i_x^p[k+2,1]\big|_{S_n^m} \\ &= D^{m1} \cdot F_{1x}[k+1]|_{S_n^m[k+1]} \\ &\quad + F_{2x}[k+1]|_{S_n^m[k+1]} \end{aligned} \tag{16}$$

where,

$$\begin{aligned} F_{1x}[k+1]|_{S_n^m[k+1]} &= \Delta i_x^{rec}[k+1,2]\big|_{S_n^{m2}[k+1]} \\ &\quad - \Delta i_x^{rec}[k+1,1]\big|_{S_n^{m1}[k+1]} \\ F_{2x}[k+1]|_{S_n^m[k+1]} &= i_x^*[k+2,1] - i_x[k,1]|_{S_n^{m2}[k-1]} \\ &\quad - \Delta\, i_x^{rec}[k]\big|_{S_n^m[k]} \\ &\quad - \Delta\, i_x^{rec}[k+1,2]\big|_{S_n^{m2}[k+1]} \end{aligned}$$

From the above expression, it can be observed that the influence of the application time ratio is significantly proportional to the calculation of the current error value of the $(k+2)$th sampling time. The cost function is obtained as:

$$\begin{aligned} g[k+2]|_{S_n^m} &= \left|E_\alpha[k+2]|_{S_n^m}\right| + \left|E_\beta[k+2]\big|_{S_n^m}\right| \\ &= \Big|D^{m1} \cdot F_{1\alpha}[k+1]|_{S_n^m[k+1]} \\ &\quad + F_{2\alpha}[k+1]|_{S_n^m[k+1]}\Big| \\ &\quad + \Big|D^{m1} \cdot F_{1\beta}[k+1]|_{S_n^m[k+1]} \\ &\quad + F_{2\beta}[k+1]\big|_{S_n^m[k+1]}\Big| \end{aligned} \tag{17}$$

The design of the application time ratio of the modulated module predictive current controller with online duty cycle calculation is to simplify the method of calculating the existing modulation strategy. The cost function of the existing modulation strategy method takes the form of the sum of squares, and the application time proportion is obtained by performing partial differentiation of the cost function. The absolute minimum value of the cost function must occur for any application time proportion, where the partial derivative of the time proportion is equal to zero for any applied time. In order to simplify the calculation, the proposed method with online duty cycle calculation has discussed the concept of applying time ratio proportion, which is different from the existing methods. The design description for the online duty ratio calculation is given in the following discussions.

According to the definition of the current error equation in (16), the physical meaning of the current error is the current command minus the predicted value of the stator current, and the cost function is based on the relative minimum value of the current error designed for the controller. Therefore, to obtain the best application time ratio, the absolute value of the cost function is first set to zero and is given as:

$$g[k+2]|_{S_n^m} = \left|E_\alpha[k+2]|_{S_n^m}\right| + \left|E_\beta[k+2]\big|_{S_n^m}\right| = 0 \tag{18}$$

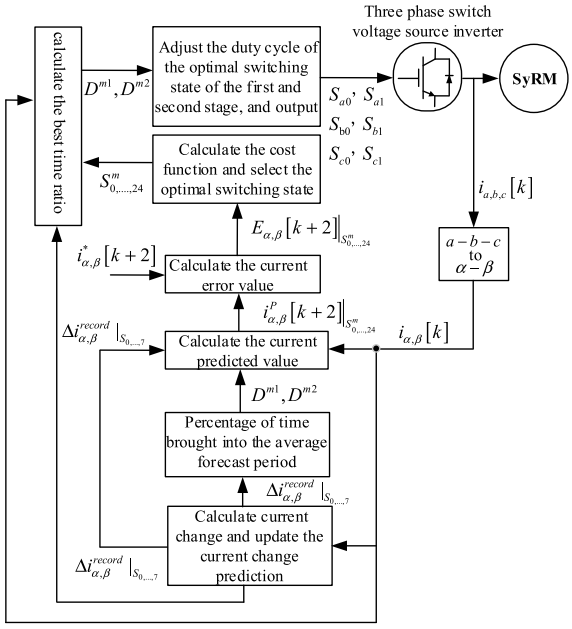

FIGURE 5. Block diagram of the modulated DVV MFPCC with the calculation of online duty cycle.

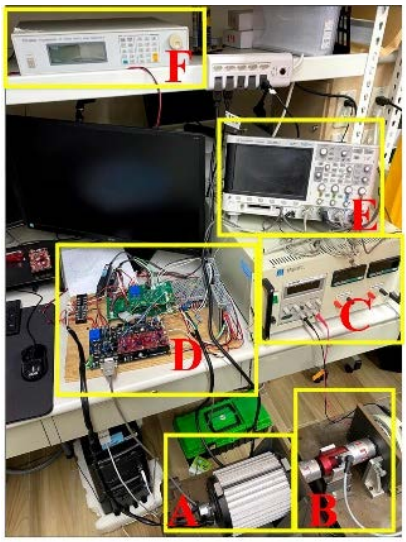

FIGURE 6. Prototype of experimental setup ((A) synchronous reluctance motor; (B) dynamometer; (C) dynamometer control unit; (D) drive circuit; (E) digital storage oscilloscope; (F) DC power supply).

$$\begin{aligned} g[k+2]|_{S_n^m} &= \Big|D^{m1} \cdot F_{1\alpha}[k+1]|_{S_n^m[k+1]} \\ &\quad + F_{2\alpha}[k+1]|_{S_n^m[k+1]}\Big| \\ &\quad + \Big|D^{m1} \cdot F_{1\beta}[k+1]|_{S_n^m[k+1]} \\ &\quad + F_{2\beta}[k+1]\big|_{S_n^m[k+1]}\Big| \\ &= 0 \end{aligned} \tag{19}$$

By rearranging the above expressions, the application time ratio found in the cost function at $(k+1)$th sampling period

TABLE 2. Synchronous reluctance motor parameters.

Motor Parameters	Values
Number of poles	4 pole
Rated power	500 W
Winding resistance	2.5 Ω
d-axis inductance (L_d)	48.19 mH
q-xis inductance (L_q)	24.5 mH
Motor shaft inertia	0.0183 kg-m^2
Motor shaft friction coefficient	0.0063 Nm-sec/rad
Rated speed	1500 rpm

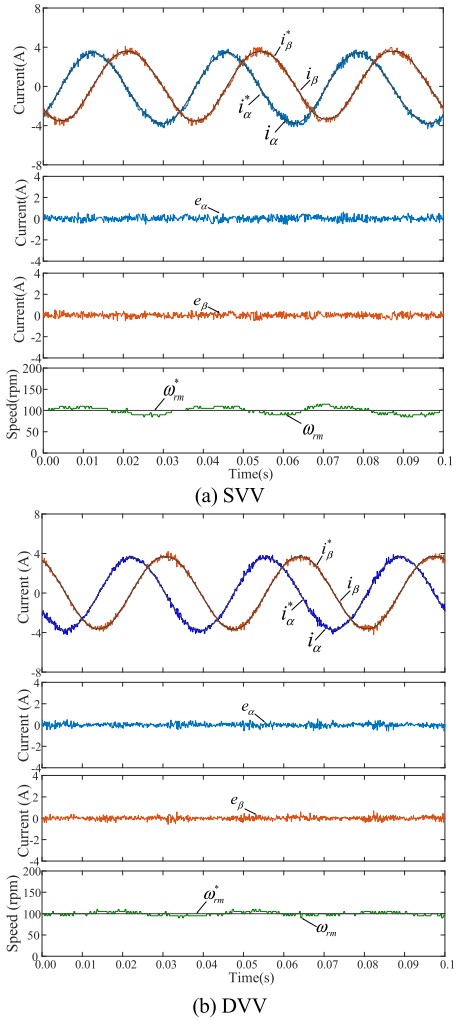

(a) SVV

(b) DVV

FIGURE 7. Measured graph in steady-state at a speed command of 100 rpm and an external load torque of 1 Nm.

can be obtained accordingly as:

$$D^{m1} = \frac{\left(-F_{2\alpha}[k+1]|_{S_n^m[k+1]} - F_{2\beta}[k+1]\big|_{S_n^m[k+1]}\right)}{\left(F_{1\alpha}[k+1]|_{S_n^m[k+1]} + F_{1\beta}[k+1]\big|_{S_n^m[k+1]}\right)} \tag{20}$$

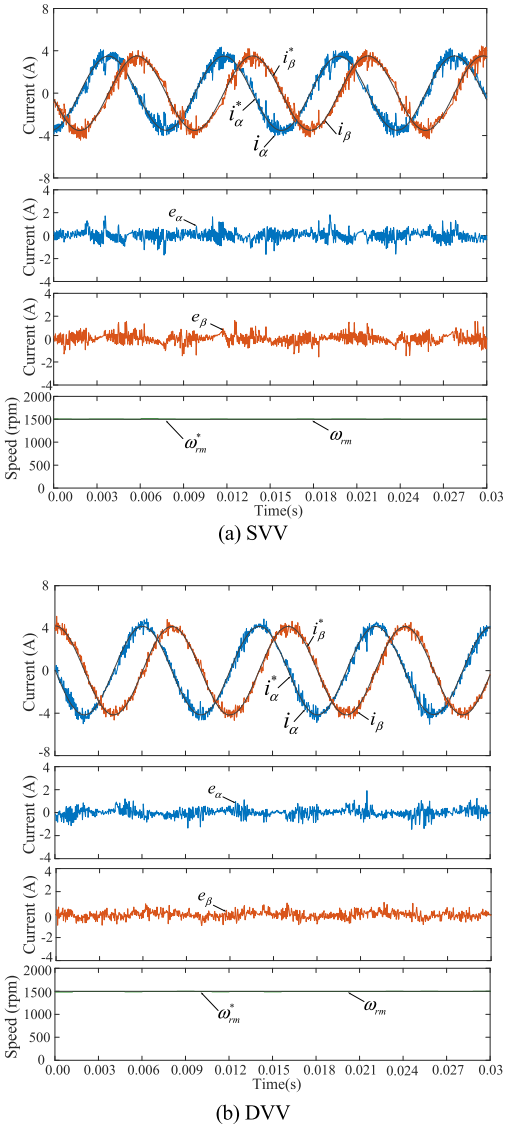

(a) SVV

(b) DVV

FIGURE 8. Measured graph in steady-state at a speed command of 1500rpm and an external load torque of 1 Nm.

If the application time ratio satisfies the upper and lower limits of (2), it can become the best optimized application time ratio and is given as:

$$D^{m1}_{opt} = D^{m1} \tag{21}$$

The subscript symbol "*opt*" for the time proportion is the abbreviation of optimization; D^{m1}_{opt} represents the first modulated application time based on the online duty cycle calculation for two applied voltage vectors. Based on the application time ratio obtained, the application time of the second applied voltage vector can be calculated using the mathematical relation of duty ratios in (2). If the application time ratio exceeds the limit given in (2), then the application time ratio of the first switching state of the (k + 1)th time be the upper limit; if less than the lower limit, then the application time ratio is set to a lower limit. The current predicted value at $(k + 2)$th

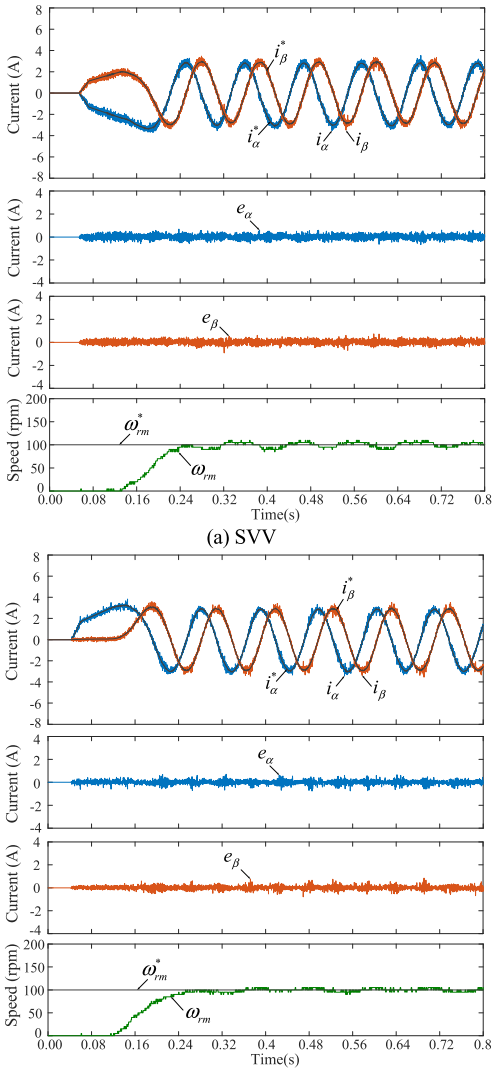

FIGURE 9. Measured graph from a standstill position of the motor to steady-state setting under a speed command of 100rpm and load 0.6 Nm.

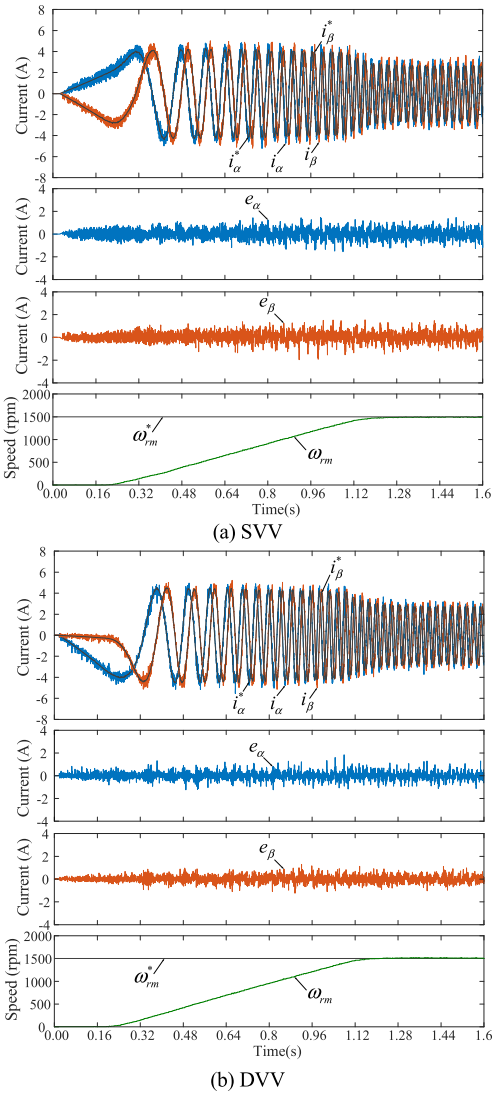

FIGURE 10. Measured graph from a standstill position of the motor to the steady-state setting under a speed command 1500rpm and load 0.6 Nm.

can be obtained using the application time ratio, which is used to calculate the cost function of each group. After obtaining the total cost function of 25 modulated switching states, the switching combination corresponding to the relative minimum value of the cost function is selected as given below:

$$g[k+2]|_{S^m_{n,opt}} = \min S^m_n, \quad S^m_n \in \{S^m_0, S^m_1, \ldots\ldots\ldots, S^m_{24}\} \tag{22}$$

The application time ratio of the first and second applied switching states is used to modulate the voltage vector and output to the inverter to complete the dual-voltage-vector modulation type MFPCC for the next k th online duty cycle calculation. Fig. 5 shows the block diagram of the dual-vector modulation model-free predictive current controller system for the calculation of the online duty cycle. The figure shows the complete structure of the proposed modulated DVV for the SynRM drive system.

III. PRACTICAL VALIDATION AND PERFORMANCE EVALUATION OF THE PROPOSED METHOD

In order to validate the proposed method practically on the synchronous reluctance motor, a laboratory prototype is developed and is shown in Fig. 6. The hardware setup helps to verify the tracking performance, feasibility, and correctness of the proposed online duty cycle modulated dual-voltage-vector MFPCC. The test setup includes a synchronous reluctance motor, drive circuit, oscilloscope, DC power supply, and measuring equipment to validate the proposed method. The drive circuit consists of an IGBT power module, Texas Instruments digital signal processor TMS320F28379D, over current protection, drive signal isolation circuit, analog to digital converter, current/voltage conversion circuit, and current sensors. The parameters of the synchronous reluctance

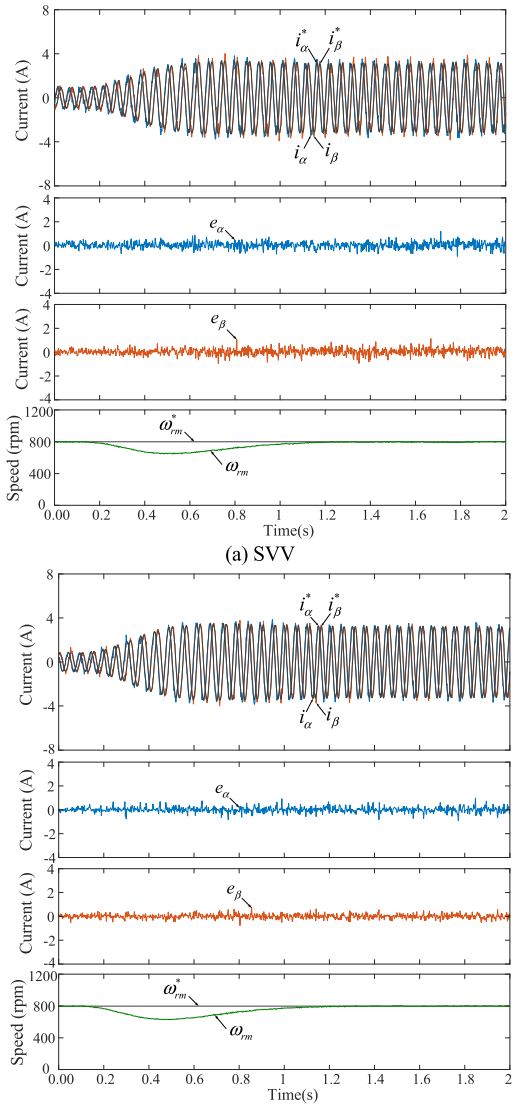

FIGURE 11. Measured graph from a no load to 1 Nm at a constant speed command of 800rpm.

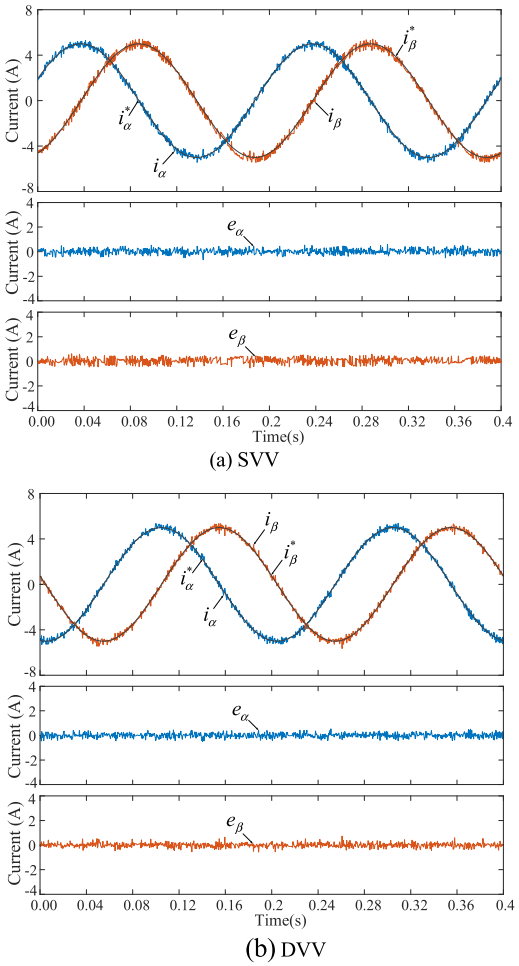

FIGURE 12. Steady-state results at a current command peak value of 5A and a operating frequency of 10Hz.

motor are shown in Table 2. In addition to the proposed method, conventional single-voltage-vector MFPCC is also implemented for comparison purposes. Both methods are realized with the same experimental setup, and a detailed comparison study is performed. The control processor uses a sampling time of 75μs for implementing the experimental studies. By the way, the six power switches in the three-phase voltage source inverter operate at variable switching frequencies due to the design of the modulated DVV.

The experimental studies are carried out during steady state and dynamic conditions. The reluctance motor is operated under different speed conditions during steady-state operation. Fig. 7 and Fig. 8 show the steady-state speed and current tracking performance of SynRM, having an external load of 1 Nm with different speed conditions for both DVV and SVV MFPCCs. The α-axis and β-axis current command values are kept at 4 A, and the actual currents follow the commanded values. With the implementation of DVV MFPCC, the current error is reduced and tracks the commanded speed quickly, compared to SVV MFPCC. Fig. 9 and Fig. 10 show the experimental studies performed during the motor accelerating from a standstill condition to the rated speed command. The change in motor speed can be observed from 0 to 100 rpm in Fig. 9 and 0 to 1500 rpm in Fig. 10. It can be observed that the DVV MFPCC scheme improves the current tracking performance at a lesser current error compared to the SVV MFPCC. Compared to the low-speed condition, the current tracking performance at high speed deteriorated due to large and pulsating load currents.

Fig. 11 shows the motor is loaded from 0 Nm to 1 Nm instantaneously after 0.2 sec. From the experimental studies, the adaptability of the PI speed controller will significantly affect the current tracking effect of the predicted current controller. The proposed DVV modulation method shows better current tracking performance than SVV modulation.

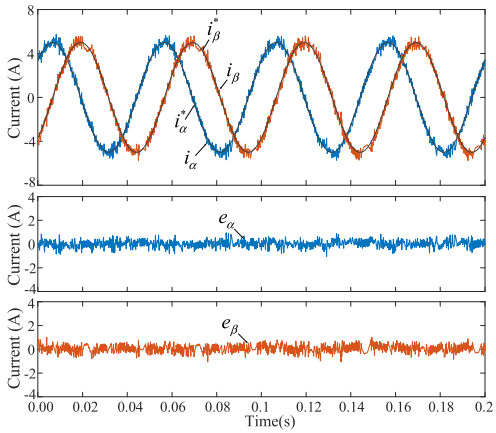

(a) SVV

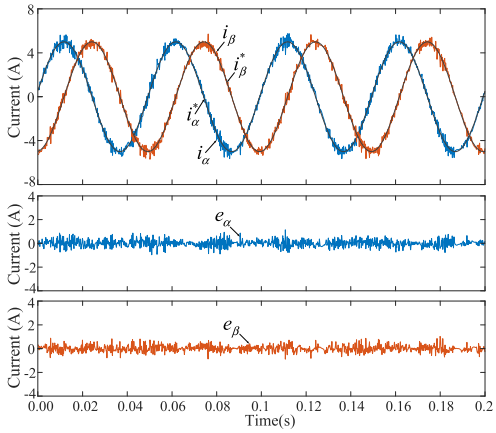

(b) DVV

FIGURE 13. Steady state results at a current command peak value of 5A and operating frequency of 30Hz.

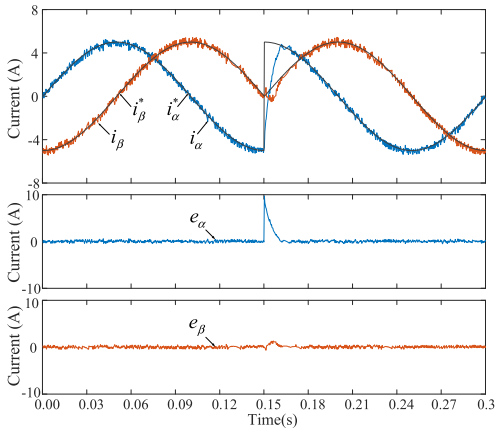

(a) SVV

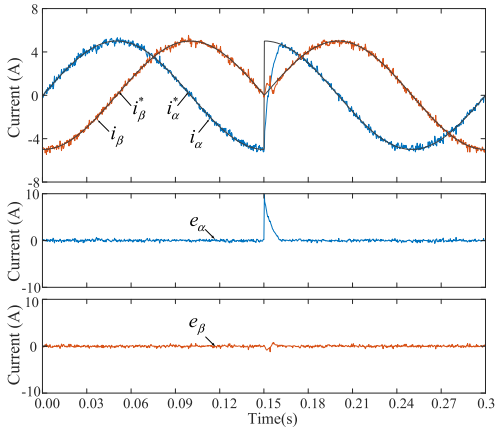

(b) DVV

FIGURE 14. A step change in the current command from −5 A to 5 A.

TABLE 3. Quantitative analysis of experimental studies.

Figure	MFPCC strategy	Average current error (A)		Current ripple (A)	
		α – axis	β-axis	α – axis	β-axis
7	SVV	0.1653	0.157	0.2073	0.1934
	DVV	0.1244	0.1207	0.163	0.1566
8	SVV	0.3279	0.3374	0.4324	0.4393
	DVV	0.2729	0.2429	0.3714	0.3128
9	SVV	0.1423	0.1397	0.1842	0.177
	DVV	0.1129	0.1055	0.1543	0.1438
10	SVV	0.2852	0.2789	0.3688	0.3675
	DVV	0.2079	0.1928	0.2861	0.2596
11	SVV	0.2083	0.2119	0.2658	0.2711
	DVV	0.1568	0.1381	0.2173	0.1821
12	SVV	0.1599	0.1902	0.1981	0.2303
	DVV	0.1374	0.1311	0.1751	0.1705
13	SVV	0.2561	0.2823	0.3181	0.343
	DVV	0.2306	0.2068	0.2977	0.2745
14	SVV	0.2932	0.2006	0.8484	0.2652
	DVV	0.2553	0.1381	0.8215	0.1904
15	SVV	0.2729	0.2716	0.341	0.334
	DVV	0.2145	0.2108	0.284	0.287

Fig. 12 and Fig. 13 show the steady-state experimental results of DVV and SVV MFPCCs for different frequency conditions. The current tracking for the DVV MFPCC shows better performance compared to SVV MFPCC. Furthermore, one can observe that the lower the current frequency, the better the current tracking effect. The transient performance of the proposed method is also validated by applying a step change in the current value. A step change in current of −5A to 5A is applied after 0.15s and is shown in Fig. 14. The performance of the current tracking is improved in DVV MFPCC compared to SVV MFPCC. The current error is also observed to reduce. The performance of the proposed scheme is also validated by changing the frequency from 10Hz to 30Hz and back to 10Hz again, as shown in Fig. 15.

From the above experimental studies, the increased number of vectors in a switching cycle improves the current tracking performance and reduces the current error. Due to the implementation of the online duty cycle modulation method, the calculation time is reduced and also has excellent current tracking performance. A quantitative analysis of the above experimental results is given in Table 3. The average current error and current ripple are given in Table 3. The quantitative results show that the proposed method's average current error and current ripple are lesser than the conventional single-voltage vector.

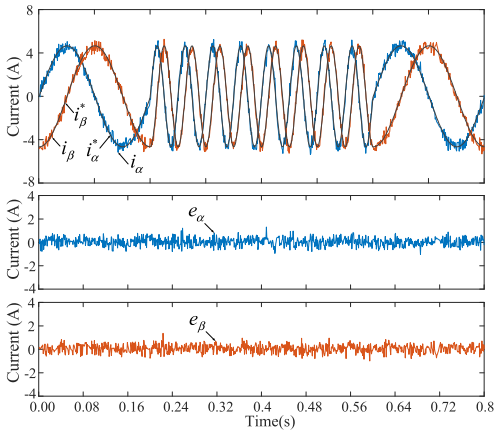

(a) SVV

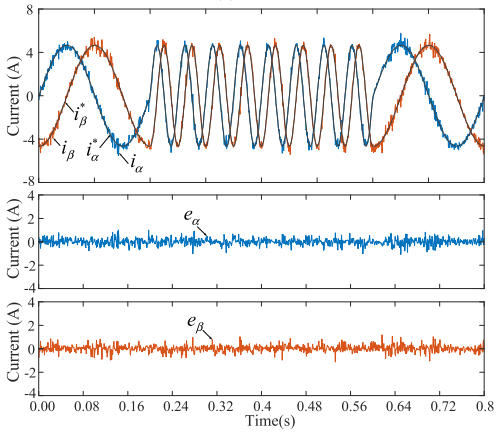

(b) DVV

FIGURE 15. A step change in frequency from 10Hz to 30Hz and 30Hz to 10Hz.

IV. CONCLUSION

A modulated dual-voltage-vector MFPCC with online duty cycle calculation for SynRM drive is proposed in this article. The developed online duty ratio calculation method simplifies the problem of cost function optimization. The average duty ratio is initially considered, and the online duty ratio is calculated in the next switching cycle. The proposed method reduces the current ripples and current errors that generally exist in the conventional SVV MFPCC. It also reduces the calculation time and tracks the current effectively. Finally, experimental studies were performed on a laboratory prototype using the microcontroller TMS320F28379D. The experimental results during steady-state and transient conditions show the effectiveness and feasibility of modulating the predictive current controller with online duty cycle calculation.

REFERENCES

[1] C.-K. Lin, J.-T. Yu, Y.-S. Lai, and H.-C. Yu, "Improved model-free predictive current control for synchronous reluctance motor drives," *IEEE Trans. Ind. Electron.*, vol. 63, no. 6, pp. 3942–3953, Jun. 2016, doi: 10.1109/TIE.2016.2527629.

[2] B. Wang, J. Hu, and W. Hua, "Design process of a triple redundant fault tolerant PMA SynRM," *IEEE Access*, vol. 7, pp. 76241–76249, 2019, doi: 10.1109/ACCESS.2019.2920627.

[3] B. Nikmaram, S. A. Davari, P. Naderi, C. Garcia, and J. Rodriguez, "Sensorless simplified finite control set model predictive control of SynRM using finite position set algorithm," *IEEE Access*, vol. 9, pp. 47184–47193, 2021, doi: 10.1109/ACCESS.2021.3068085.

[4] T. Liu, H. S. Haslim, and S. Tseng, "Predictive controller design for a high-frequency injection sensorless synchronous reluctance drive system," *IET Electr. Power Appl.*, vol. 11, no. 5, pp. 902–910, May 2017, doi: 10.1049/iet-epa.2016.0054.

[5] C. Li, G. Wang, G. Zhang, D. Xu, and D. Xiao, "Saliency-based sensorless control for SynRM drives with suppression of position estimation error," *IEEE Trans. Ind. Electron.*, vol. 66, no. 8, pp. 5839–5849, Aug. 2019, doi: 10.1109/TIE.2018.2874585.

[6] K.-C. Kim, J. S. Ahn, S. H. Won, J.-P. Hong, and J. Lee, "A study on the optimal design of SynRM for the high torque and power factor," *IEEE Trans. Magn.*, vol. 43, no. 6, pp. 2543–2545, Jun. 2007, doi: 10.1109/TMAG.2007.893302.

[7] J. Rodriguez and P. Cortes, *Predictive Control of Power Converters and Electrical Drives*, 1st ed. West Sussex, U.K.: Wiley, 2012, pp. 133–143.

[8] T. Tarczewski and L. M. Grzesiak, "Constrained state feedback speed control of PMSM based on model predictive approach," *IEEE Trans. Ind. Electron.*, vol. 63, no. 6, pp. 3867–3875, Jun. 2016, doi: 10.1109/TIE.2015.2497302.

[9] S. Kouro, P. Cortes, R. Vargas, U. Ammann, and J. Rodriguez, "Model predictive control—A simple and powerful method to control power converters," *IEEE Trans. Ind. Electron.*, vol. 56, no. 6, pp. 1826–1838, Jun. 2009, doi: 10.1109/TIE.2008.2008349.

[10] J. Rodriguez, J. Pontt, C. A. Silva, P. Correa, P. Lezana, P. Cortes, and U. Ammann, "Predictive current control of a voltage source inverter," *IEEE Trans. Ind. Electron.*, vol. 54, no. 1, pp. 495–503, Feb. 2007, doi: 10.1109/TIE.2006.888802.

[11] H. Hadla and S. Cruz, "Predictive stator flux and load angle control of synchronous reluctance motor drives operating in a wide speed range," *IEEE Trans. Ind. Electron.*, vol. 64, no. 9, pp. 6950–6959, Sep. 2017, doi: 10.1109/TIE.2017.2688971.

[12] A. Farhan, M. Abdelrahem, C. M. Hackl, R. Kennel, A. Shaltout, and A. Saleh, "Advanced strategy of speed predictive control for nonlinear synchronous reluctance motors," *Machines*, vol. 8, no. 3, p. 44, Aug. 2020, doi: 10.3390/machines8030044.

[13] W. Tu, G. Luo, R. Zhang, Z. Chen, and R. Kennel, "Finite-control-set model predictive current control for PMSM using grey prediction," in *Proc. IEEE Energy Convers. Congr. Expo. (ECCE)*, Sep. 2016, pp. 18–22, doi: 10.1109/ECCE.2016.7855117.

[14] R. Yang, M.-Y. Wang, L.-Y. Li, C.-M. Zhang, and J.-L. Jiang, "Robust predictive current control with variable-gain adaptive disturbance observer for PMLSM," *IEEE Access*, vol. 6, pp. 13158–13169, 2018, doi: 10.1109/ACCESS.2018.2809608.

[15] M. Yang, X. Lang, J. Long, and D. Xu, "Flux immunity robust predictive current control with incremental model and extended state observer for PMSM drive," *IEEE Trans. Power Electron.*, vol. 32, no. 12, pp. 9267–9279, Dec. 2017, doi: 10.1109/TPEL.2017.2654540.

[16] X. Sun, Y. Zhang, G. Lei, Y. Guo, and J. Zhu, "An improved deadbeat predictive stator flux control with reduced-order disturbance observer for in-wheel PMSMs," *IEEE/ASME Trans. Mechatronics*, vol. 27, no. 2, pp. 690–700, Apr. 2022, doi: 10.1109/TMECH.2021.3068973.

[17] C.-K. Lin, T.-H. Liu, J.-T. Yu, L.-C. Fu, and C.-F. Hsiao, "Model-free predictive current control for interior permanent-magnet synchronous motor drives based on current difference detection technique," *IEEE Trans. Ind. Electron.*, vol. 61, no. 2, pp. 667–681, Feb. 2014, doi: 10.1109/TIE.2013.2253065.

[18] P. G. Carlet, F. Tinazzi, S. Bolognani, and M. Zigliotto, "An effective model-free predictive current control for synchronous reluctance motor drives," *IEEE Trans. Ind. Appl.*, vol. 55, no. 4, pp. 3781–3790, Jul./Aug. 2019, doi: 10.1109/TIA.2019.2910494.

[19] C. A. Agustin, J.-T. Yu, C.-K. Lin, J. Jai, and Y.-S. Lai, "Triple-voltage-vector model-free predictive current control for four-switch three-phase inverter-fed SPMSM based on discrete-space-vector modulation," *IEEE Access*, vol. 9, pp. 60352–60363, 2021, doi: 10.1109/ACCESS.2021.3074067.

[20] L. Tarisciotti, P. Zanchetta, A. Watson, S. Bifaretti, and J. C. Clare, "Modulated model predictive control for a seven-level cascaded H-bridge back-to-back converter," *IEEE Trans. Ind. Electron.*, vol. 61, no. 10, pp. 5375–5383, Oct. 2014, doi: 10.1109/TIE.2014.2300056.

[21] X. Sun, T. Li, Z. Zhu, G. Lei, Y. Guo, and J. Zhu, "Speed sensorless model predictive current control based on finite position set for PMSHM drives," *IEEE Trans. Transport. Electrific.*, vol. 7, no. 4, pp. 2743–2752, Dec. 2021, doi: 10.1109/TTE.2021.3081436.

[22] X. Sun, T. Li, M. Yao, G. Lei, Y. Guo, and J. Zhu, "Improved finite-control-set model predictive control with virtual vectors for PMSHM drives," *IEEE Trans. Energy Convers.*, vol. 37, no. 3, pp. 1885–1894, Sep. 2022, doi: 10.1109/TEC.2021.3138905.

[23] P. Cortes, J. Rodriguez, C. Silva, and A. Flores, "Delay compensation in model predictive current control of a three-phase inverter," *IEEE Trans. Ind. Electron.*, vol. 59, no. 2, pp. 1323–1325, Feb. 2012, doi: 10.1109/TIE.2011.2157284.

VENKATA R. REDDY was born in Andhra Pradesh, India, in 1991. He received the B.Tech. degree in electrical and electronics engineering from the Annamacharya Institute of Technology and Sciences, Rajampeta, India, in 2012, and the M.Tech. degree in computational engineering from the Rajiv Gandhi University of Knowledge Technologies, Kadapa, India, in 2015, and the Ph.D. degree in electrical engineering from the Department of Electrical and Electronics Engineering, National Institute of Technology Goa, Ponda, India. He was a Postdoctoral Research Fellow with the Department of Electrical Engineering, National Taiwan Ocean University, Keelung, Taiwan. He is currently working as an Assistant Professor with the Department of Electrical and Electronics Engineering, SRM University, Amaravati, India. His research interests include renewable energy systems, and power electronic for grid connected and motor drive applications.

CRESTIAN ALMAZAN AGUSTIN (Graduate Student Member, IEEE) was born in Isabela, Philippines, in 1989. He received the B.S. degree in electrical engineering from Isabela State University, Ilagan, Philippines, in 2012, the M.S. degree in engineering management from the University of La Salette, Santiago, Philippines, in 2015, the M.S. degree in electrical engineering from the University of Saint Louis, Cagayan, Philippines, in 2017, and the Ph.D. degree in electrical engineering from the National Taiwan Ocean University, Keelung, Taiwan, in 2022. From 2014 to 2017, he was a Resident Engineer with the SM Engineering Design and Development, Pasay, Philippines. He is currently a Lecturer with the Department of Electrical Engineering, Isabela State University. His research interests include control of motor drives and inverter topologies.

CHENG-KAI LIN was born in Taipei, Taiwan, in 1980. He received the B.S. degree in electrical engineering from the Ming Chi University of Technology, Taipei, in 2002, and the M.S. and Ph.D. degrees in electrical engineering from the National Taiwan University of Science and Technology, Taipei, in 2004 and 2009, respectively. From October 2009 to August 2012, he was a Postdoctoral Researcher with the Department of Electrical Engineering, National Taiwan University, Taipei. He is currently an Associate Professor of electrical engineering with the National Taiwan Ocean University, Keelung, Taiwan. His research interests include motor drive control, power electronic applications, and control applications.

JUNG-CHIEH CHEN was born in Taichung, Taiwan, in 1995. He received the B.S. degree in systems engineering and naval architecture and the M.S. degree in electrical engineering from the National Taiwan Ocean University, Keelung, Taiwan, in 2019 and 2021, respectively. His research interest includes motor drive control and applications.